An Assessment of Potential Hazards to the Cassini Spacecraft from Debris along Satellite Orbits

Joseph A. Burns, Robert A. Kolvoord
and Douglas P. Hamilton

Cornell University

Report to Cassini Project
August 1989

Introduction

The Cassini spacecraft, which is to orbit Saturn for almost four years during the early part of the next century, is designed to be captured when its engines fire deep within the planet's magnetosphere. Many of the spacecraft's subsequent traverses through the planet's equatorial plane will occur close to satellite orbit paths in order to permit various high–resolution observations of the satellites [see Cassini: Report on the Phase A Study, ESA and NASA Document SCI (88)5, October 1988]. In addition, early in the mission the spacecraft will fly along a low inclination path passing over many satellite orbits. Questions have arisen over the years as to whether regions near the satellites are likely to be unusually safe (the simple argument going that the satellites themselves have swept such regions clear) or abnormally hazardous (the point being that, at least for an isolated three–body system, orbits in this locale are the only ones that can possibly be stable).

We provide here a preliminary discussion of the likely risk to be faced by a spacecraft passing near the satellite orbits. We start by summarizing the evidence for material in orbit near the satellites; this includes direct observations of co–orbiting moons and dust as well as indirect clues for debris clouds as inferred from charged particle absorption signatures. Following this précis, we consider two different approaches to the problem. First, we recall theoretical results from the classical circular restricted three–body problem as to the circumstances under which orbits are stable versus when they are chaotic; we then illustrate these orbital classes by a numerical simulation that is generalized by showing how it scales for the relevant Saturnian satellites. Second, using arguments coming from theoretical studies of magnetospheric absorption by rings and satellites, we are able to place some very weak constraints on the nature of the material that is thought to be responsible for the observed depletion of charged particles.

Evidence for Debris Sharing Satellite Orbits

The Saturnian satellite system contains several examples of objects sharing one another's orbits (Burns 1986). Ground–based observations made a decade ago found Lagrangian satellites in Saturn's environs: there are two moonlets in the orbit of Tethys

(4.88 R_s, where R_s is the Saturnian radius or 60 330 km) and a companion to Dione (6.26 R_s). Similar telescopic studies also provided equivocal evidence, which was confirmed and clarified by spacecraft measurements, for the co–orbital satellites Janus and Epimetheus (2.51 R_s). Neither of these dynamical configurations is known in any other satellite system. Several other satellites, including a Lagrangian compatriot to Enceladus (3.95 R_s), may have also been seen by the Voyager spacecraft but observations are not conclusive.

Not all material in satellite orbits is palpable since there is convincing circumstantial evidence for the presence of additional material along or near satellite orbits. This evidence comes in the form of "microsignatures" (radially narrow, abrupt and substantial depletions of energetic charged particles) noted by the Pioneer and Voyager spacecraft as they passed beneath the orbits of several inner Saturnian moons (Van Allen 1984; Carbary et al. 1983) and near the F ring (Simpson et al. 1980, Van Allen 1982, Cuzzi and Burns 1988). The abruptness, location and width of the depletions indicate that known satellites do not cause these absorptions and so longitudinally fragmented clumps of particulate matter with low optical depth (10^{-2}–10^{-4}) are suspected. For example, the most complete study of an anomalous satellite absorption signature is that by Chenette and Stone (1983) who, following Simpson et al. (1980), claimed that measurements made in the vicinity of Mimas could be explained by a localized tenuous cloud of debris.

The microsignatures observed by the Pioneer and Voyager spacecraft as they passed near the major inner Saturnian satellites are summarized in Table I. The three spacecraft traversed a total of 26 satellite orbits (3 spacecraft with 2 passes/orbit of 5 moons equals 30 passes but Voyager 1 did not get as far as Mimas and Enceladus) and detected 7 events of which at least 4 are generally ascribed to absorption by the satellite. The three unexplained events include detections at Mimas by inbound Pioneer 11 and outbound Voyager 2 (Simpson et al. 1980; Vogt et al. 1982; Carbary et al. 1983; Chenette and Stone 1983) and another detection at Enceladus by inbound Voyager 2 (Vogt et al. 1982; Carbary et al. 1983).

The microsignature at the orbit of Mimas discovered by Pioneer 11 has been attributed by Simpson et al. (1980) to a companion satellite (or a localized distribution of dust) near Mimas's trailing Lagrangian point whereas, because of a different interpretation of the precise particles being measured, Van Allen et al. (1980) interpret it as caused by Mimas itself. The Voyager 2 detection near Mimas's orbit is generally acknowledged to be due to something other than the satellite (Chenette and Stone 1983). The Enceladus microsignature is somewhat puzzling because i.) it was detected in both protons and low energy electrons (which drift in different directions), implying the absorber must have been directly above; and ii.) the absorptions of particles with widely differing energy and species are very similar (about 2640 km wide with a maximum depletion of ~ 35%) even though gyroradii and especially absorbtivities are quite different. As already stated, the other four absorptions are believed to be caused by the satellites, which were nearby, although all have some problematic aspects (Van Allen 1984, Carbary et al. 1983).

A final bit of evidence for coorbital debris comes from the Voyager 1 plasma wave instrument when the spacecraft pierced Dione's "clear zone" (Gurnett et al. 1981). Because of contamination of the plasma wave data by signals from other phenomena, no characteristics of the causative particles have been ascertained thus far although clearly some dust was detected (D.A. Gurnett, private communication, August 1989).

Constraints from Celestial Mechanics

The restricted three–body problem, perhaps the most celebrated of all in classical mechanics, may suggest circumplanetary regions in which material might be found. In the circular restricted problem, where an infinitesimal mass moves under the action of two other objects that orbit one another on circular paths, motions near the two "Lagrangian triangular points" (located leading the smaller mass by 60° and trailing it by an equal angle; see Fig. 1) can be stable. [All results are described in a reference frame that rotates with the orbital motion of the primaries.] Expressing the ratio between the smaller primary's mass and the total system mass as μ, stability occurs for $\mu < 0.0385$, a condition easily satisfied by Saturn and all its satellites. This stability remains true for small orbital eccentricities.

A sketch of the problem and the nature of the expected stable orbits is shown in Figure 1. Directly below, simplified analytical expressions for the various regions are given in terms of μ and R (the orbital distance to Saturn). Table II lists values for the sizes of these regions for specific Saturnian satellites and for a hypothetical object for which trajectories are plotted. This is followed by some diagrams of typical trajectories for the problem.

Stable orbits in the shapes of tadpoles encircle the triangular points (see Fig. 1). The radial separation of tadpoles from the triangular Lagrange point is, from Dermott and Murray (1981), $2\left[\frac{\beta-h}{3}\right]^{1/2} \mu^{1/2}R$; β and h come from the precise trajectory that is considered but generally are between 3 and 5. For definiteness in Table II we choose β–h =1; thus $\Delta r_T \approx 1.15\ \mu^{1/2}R$.

Another class of stable orbits are horseshoe–shaped in the rotating frame, enclosing both triangular points (see Fig. 1). The radial separation of horseshoes is $2(\alpha/3)^{1/2}\mu^{1/3}R$ where, for symmetric paths, $0 < \alpha \lesssim 0.4$ with lower values corresponding to orbits that more and more closely duplicate the satellite's path (see Dermott and Murray 1981). For simplicity in Table II, we choose $\alpha = 3/16$; thus $\Delta r_H \leq 0.5\mu^{1/3}R$.

An analytical expression is also available for the longitudinal separation of the tips of symmetric horseshoe orbits from the satellite. As can be seen on trajectory plots, material does pass through the gap between these symmetric horseshoes and the satellite but paths in that region are either chaotic orbits or horseshoes that have a measurable induced eccentricity following a satellite encounter. As will be argued, at least the first class of these is likely to be ultimately eliminated from the coorbital region; thus the computed separation should indicate a zone depleted in material. From Dermott and Murray (1981), the longitudinal separation is $y_{min} = \left[\frac{8}{3\Delta a_o^2}\right]\mu R$, where Δa_o is the initial radial distance between the horseshoeing particle and the satellite. Now $\Delta a_o = 2(\alpha/3)^{1/2}\mu^{1/3}$

so, for $\alpha \lesssim 1/3$, $y_{min} \gtrsim 6\mu^{1/3}R$ or twelve times Δr_H. This gap, in which co–orbiting particles cannot approach the satellite, may be an eminently suitable locale to target flybys.

Particles whose orbits are radially more distant from the Lagrange points than these stable orbits move past the satellite. Those particles that approach the satellite closely are scattered so that the final outcome can depend sensitively on the precise fly–by distance. Chaotic orbits should reside within ~ $1.3\mu^{2/7}R$ according to a postulate of Wisdom (1980) that has recently been numerically confirmed to within 15% by Duncan et al. (1989). In our experience, this over–estimates the chaos zone by a factor of 2, perhaps because we have considered only a single pass whereas the criterion is based on many (~ 10^3) flybys. It seems likely that orbits in this chaotic regime may be removed from the system either by ejection or, more probably, by collision with the satellite. At distances beyond this chaotic regime, particles drift past the satellite and have their orbital eccentricities and semimajor axes slightly modified (Showalter and Burns 1982). Small moonlets embedded within a coorbital ring will do little to alter these results because their synodic periods are so long (Kolvoord and Burns 1987).

Trajectory Plots

Trajectories of particles moving past a small satellite, itself in a circular orbit, are shown in Figs. 2–7 as seen in a frame moving with the satellite. Particles are started on circular orbits far from the satellite; as they drift past the satellite (due to the difference in orbital speed as a function of distance from the primary), they are perturbed by the satellite. The three distinct orbital types discussed earlier are apparent in Fig. 2. Gravitational wakes (at top and bottom) are produced when the perturbations change circular orbits into elliptic ones; the wavelength is given by $3\pi\Delta r$ and results from the particle's synodic period (Showalter and Burns 1982). Chaotic orbits (the upper middle left and lower middle right) have passed close by the satellite. Horseshoe orbits lie on the central strip. Tadpole orbits are not seen because they lie well within the horseshoes, far off the diagram to the left and right. The breakdown into various dynamical regimes

shown in Fig. 2 is typical and the only difference for the suite of satellites is the scaling which follows the analytical rules presented above. The dynamical regimes are explicitly identified in Fig. 2; also plotted are Δr_T, Δr_H, y_{min}, etc., which are only accurate to tens of percent since the choice of parameters is not unique.

Figs. 2–4 correspond to a small satellite ($\mu = 5\times10^{-13}$ or an object of about 5 km radius and density 1.5g–cm^{-3}) embedded in the F ring. Figs. 5–7 shows results for Enceladus. Fig. 7 illustrates particle positions with a specific time interval: it is clear that horseshoe trajectories are not only spread apart after encountering the satellite but also particles along these trajectories move faster following the encounter so that they become more widely spaced: particle densities are substantially reduced within regions inward/leading the satellite and outward/trailing the satellite.

Interpretation of Dynamical Plots

From the representative plots shown, it appears likely that the chaotic region will be swept clear because of collisions with the satellite itself, with other chaotic material or with particles trapped along horseshoe orbits. Any object in the gravitational wake region may reside there for some time. It is more difficult to ascertain the fate of debris in the horseshoe region, since this material is stable at least in the ideal problem, ignoring eccentric orbits and collisions; a conservative engineering approach must presume that material could remain here. With such an attitude and Figs. 2–7 in mind, it would be prudent for the first few flybys of satellites by Cassini (until the regions can be surveyed) to choose orbits that passed through the least densely populated regions – interior to and leading the satellite, or exterior to and trailing the satellite.

Vertical Extent of Debris Clouds

The vertical extent (that normal to the orbital plane of the primaries) of any co–orbital material cannot be constrained very well theoretically or observationally. From the theoretical side, for the restricted three body problem, motion in the third dimension is always stable; hence, horseshoing particles may have stable oscillations that

allow them to project out of the orbital plane of their confining satellite.

On the observational side, no groundbased or spacecraft images are available to constrain the problem. In addition, magnetospheric studies cannot distinguish between vertically extended absorbers and planar sheets because the measured electrons always pass through the equatorial plane during their bounce motions. A few dust grains were detected by plasma instruments aboard Voyager 1 when it traversed the Dione "clear zone" but the vertical distribution of these impacts has not yet been studied (D.A. Gurnett, personal communication, August 1989).

A best guess as to the vertical extent of material could be guided by two simple ideas. First, if the grains are injected by an impact or an eruption, any initial non–circular velocity that the grains might have is equally likely to be out of the equatorial plane as to be in it: thus the initial vertical extent of the cloud should be comparable to the radial extent (a thousand km?). Second, the primary non–planar perturbations (e.g., electromagnetic or radiation forces) act most effectively on small grains so that the largest displacements should happen for the smallest (and least hazardous) particles.

Constraints from Magnetospheric Studies

As already discussed, in situ measurements that find reduced fluxes of various charged species have been interpreted to say that clouds of debris are present along or near the orbits of some inner satellites of Saturn, including Mimas and Enceladus. From the energy of the species being depleted, the size of the absorbing particles can be estimated assuming that all particles are large enough to entirely absorb the measured particles; for example, 1.5MeV electrons are stopped by ~ 0.1 – 1cm of water ice, while only 1μm of water ice is needed to halt ~ 50keV protons.

It should be noted that, to our knowledge, microsignatures such as discussed here for the Saturnian system were not detected at Jupiter nor Uranus by Pioneer or Voyager. Presumably these unique features result from the fact that Saturn's magnetic field is the

only one that is axially aligned and nearly a pure dipole. The nature of the Saturnian field means that energetic charged particles, which generally drift approximately along constant L shells, stay radially localized and thus can be effectively absorbed by tenuous and radially narrow clouds of dust. Such a situation does not prevail at Jupiter, which has a 10^{o} tilt and a highly distorted field, nor at Uranus, where the poorly explored field is tilted by 60^{o} from the rotation axis.

We now consider briefly, following the approach of Cuzzi and Burns (1988), the nature of the clouds that could cause the anomalous absorptions seen near the orbit of Enceladus. The Mimas case, which is discussed by Chenette and Stone (1983), is similar.

For Enceladus, the microsignature is best fit by an absorption of initial width w ~ 500km that has a diffusion age A = 20 (see Cuzzi and Burns' eqn. 10 and Fig. 3). Note that both low energy protons and high energy electrons, which drift in opposite directions relative to our orbiting particles, are depleted. This implies that the absorber must have been directly overhead and, if that is true, either the cloud is extended in both directions (somewhat improbable in that approximately equal absorption depths and shapes seem to have been present in all channels) or the observed absorption shape reflects the cloud's density profile rather than being due to diffusion. In either case, the modelling used by Cuzzi and Burns (1988) is suspect but – for lack of anything better – we proceed. A further implication of the similarity of proton and electron profiles is that the absorbing particles must all be generally greater than the absorption length of the most energetic particles (i.e., 1mm or greater) so that all species are absorbed equally; yet, in view of the nominal particle size distribution for E ring material (see Showalter 1989), this is improbable. Assuming that Carbary et al. (1983 Fig. 11) are counting only 1.5 MeV electrons (drift speed V_d = 9 km/sec, bounce period of 3.3 seconds for 30^{o} pitch angle), ~ 0.1 g cm^{-2} is required for significant absorption. Hence, following Cuzzi and Burns (1988, Eqns. 7 and 8), significant absorption will occur for $\tau L = 10$ km, where τ is the cloud's optical depth and L is its length. We place a crude upper bound on L from the distance to the cloud as given by the system's age: $L_{max} = \frac{AV_d w^2}{16D}$, where D is the local diffusion

coefficient for the species being measured. Hood (1985) estimates D as $10^{-8} - 10^{-9}$ R_s^2/sec at Enceladus whereas the preferred Cuzzi and Burns (1988) value at Mimas, when extrapolated to Enceladus, is 2×10^{-7} R_s^2/sec. For the latter value, $L_{max} = 5 \times 10^3$km(or a longitudinal arc length $\Delta\theta \approx 1^o$) whereas Hood's higher diffusion coefficients give $L_{max} \sim 10^5 - 10^6$km ($\Delta\theta \sim 23^o.8 - 238^o$; in the last case, of course, the signal is no longer a microsignature). For comparison, a lower bound on the cloud's length is its radial size or 2.5×10^3 km. These various L_{max} then allow τ_{min} to be estimated: 5×10^{-5}, 10^{-3}, 10^{-2}. Recalling from Showalter's work that the E ring itself reaches a maximum τ of $\sim 5 \times 10^{-6}$ (his modelled τ is divided by 2 in order to give physical cross–section), extended clouds such as these should have been readily visible – and were not – on the few long–exposure images of the E ring taken by Voyager. However these images only encompassed a small fraction of the total E ring longitudes and thus the non–detection of debris clouds by imaging is not fatal to the hypothesis.

Another issue of interest is the fractional coverage by debris clouds of each satellite orbit circumference as implied by these measurements. Now, if the microsignatures were only present directly beneath the clouds, then the coverage would be simply the fraction of detections; there would be the additional question as to whether each satellite orbit should be treated separately in terms of the statistics of detection or whether it is sufficient to consider all orbits the same. In the latter, most simple case the coverage is $\sim$ 10%. This number is a very generous upper limit in that i.) the absorption length L of the cloud is probably much less than the length to the cloud (approximately given by L_{max}) and so the fractional coverage should be reduced by L/L_{max}, which although it is small unfortunately cannot be well constrained; and ii.) more fundamentally, the interpretation of microsignatures in terms of absorbing clouds is only a plausible inference, not a certainty: the whole model may be wrong.

To summarize, the simplest explanation of the microsignatures is that some co–orbital particles large enough to absorb MeV electrons are present along the paths of the inner Saturnian satellites. Unfortunately, with the above data alone, the

characteristics of the absorbing grains cannot be well defined and thus it is not possible to provide a definitive answer to the question of Cassini's safety during those periods when the spacecraft is passing near satellite orbits. However the information contained in this report should furnish part of the necessary background to allow an informed engineering decision to be made.

References

Burns, J.A. 1986. Some background about satellites. In Satellites (J.A. Burns and M.S. Mathews, eds.), pp. 1–38. University of Arizona Press, Tucson.

Burns, J.A., M.R. Showalter and G.E. Morfill 1984. The ethereal rings of Jupiter and Saturn. In Planetary Rings (R.J. Greenberg and A. Brahic, eds.), pp. 200–272. University of Arizona Press, Tucson.

Carbary, J.F., S.M. Krimigis, and W.–H. Ip 1983. Energetic particle microsignatures of Saturn's satellites. *J. Geophys. Res.* 88, 8947–8958.

Chenette, D.L., and E.C. Stone 1983. The Mimas ghost revisited: An analysis of the electron flux and electron microsignatures observed in the vicinity of Mimas at Saturn *J. Geophys. Res.* 88, 8755–8764.

Cuzzi, J.N., and J.A. Burns 1988. Charged particle depletion surrounding Saturn's F ring: Evidence for a moonlet belt? *Icarus* 74, 284–324.

Cuzzi, J.N., J.F. Cooper, L.L. Hood and M.R. Showalter 1989. Abundance and size distribution of ring material outside of the main rings of Saturn. Report to Cassini Project.

Dermott, S.F. and C.D. Murray 1981. The dynamics of horseshoe and tadpole orbits: I. Theory. *Icarus* 48, 1–11.

Duncan, M., T. Quinn and S. Tremaine 1989. The long–term evolution of orbits in the solar system: A mapping approach. Icarus in press.

Gurnett, D.A., W.S. Kurth and F.L. Scarf 1981. Plasma waves near Saturn: Initial results from Voyager 1. Science 212, 235–239.

Hood, L.L. 1989. Radial diffusion and losses of energetic protons in the 5 to 12 R_s region of Saturn's magnetosphere. *J. Geophys. Res.* **94**, in press.

Kolvoord, R.A., and J.A. Burns 1987. The effect of embedded and shepherding satellites on a narrow ring: A numerical simulation. *BAAS* **19**, 891.

Showalter, M.R. 1989. In Cuzzi et al. (1989).

Showalter, M.R., and J.A. Burns 1982. A numerical study of Saturn's F ring. *Icarus* 52, 526–544.

Simpson, J.A., T.S. Bastian, D.L. Chenette, R.B. McKibben and K.R. Pyle 1980. The trapped radiations of Saturn and their absorption by satellites and rings. *J. Geophys. Res.* **85**, 5731–5762.

Van Allen, J.A. 1982. Findings on rings and inner satellites of Saturn by Pioneer 11. *Icarus* **51**, 509–527.

Van Allen, J.A. 1984. Energetic particles in the inner magnetosphere of Saturn. In *Saturn* (T. Gehrels and M. Matthews, Eds.). Univ. of Arizona Press, Tucson. pp. 281–317.

Vogt, R.E., D.L. Chenette, A.C. Cummings, T.L. Garrard, E.C. Stone, A.W. Schardt, J.H. Trainor, N. Lal and F.B. McDonald, 1982. Energetic charged particles in Saturn's magnetosphere: Voyager 2 results. Science **215**, 577–582.

Wisdom, J. 1980. The resonance overlap criterion and the onset of stochastic behavior in the restricted three–body problem. *Astron. Jnl.* **85**, 1122–1133.

TABLE I: KNOWN MICROSIGNATURES

Satellite	S/C and Position	Particles	Signal Properties*	Comments/Interpretations
Mimas (r ~ 195km)	$P11_{in}$:0.3°N, 56°W	MeV electrons [Simpson, VA]	w** ~ 600km, 30% reduction for > 5MeV e^-; 20% reduction for > 2.5 MeV e^-[Ca83]	coorbital material? [Simpson] or Mimas? [VA]
	$V2_{out}$:6°S,147°E	All channels[Ca] Also [V82]	low energy particles have deeper signatures w ~ 452km;20% reduction in low energy α = 80° electrons [Ca83]	coorbital material?
Enceladus (r ~ 250km	$V2_{in}$: 27°N, 20°W	All channels [Ca] Also [V82]	w ~ 2540km, 30% reduction for > 1.5MeV e^- and also in 28-43keV ions w/ α = 90°[Ca83]	not corotation wake coorbital material?
Tethys (r ~ 530km)	$V2_{out}$: 19°S, ± 1°	All channels [Ca] Also [V82]	w ~ 980km, 50% reduction in 26-37keV e^-; 30% reduction in 37-70keV e^- [Ca83]	Tethys (?) but displaced 0.1R_S
Dione (r ~ 575km)	$V1_{out}$:0°N,25°E	26-70keV e^-[Ca]	w ~ 2300km, 40% reduction in 26-37keV e^- 15% reduction in 37-70keV e^- [Ca83]	corotation wake? of Dione

	$V2_{in}$:27°N,93°E	22-35 keV e^-[Ca]	w = [500-1000km], much smaller than V1 width 25% reduction in 22-35 keV e^- [Ca83]	coorbital material? (but only seen in one detector) Lagrange satellite 1980S6?
Rhea (r ~ 765km)	$V1_{out}$:8°N,3°E	37-200keV e^- (very strong in 500keV) [V81] [Ca]	w ~ 2280km;>75% reduction in 26-37keV e^- 40-1050keV ions [Ca83]	Rhea but displaced by $0.3R_S$(?)

* Peak heights are accurate to ~ 10%

**Widths are fairly accurate, except for Dione V2 inbound signature for which the spacecraft orbital velocity was not given

Ca = Carbary et al.

VA = Van Allen

V = Vogt et al.

Ch = Chenette and Stone

Table II: Dynamical Regimes for Saturnian Satellites

Satellite	Mass* [10^{20} kg]	μ*	Orbital* Radius R [10^3km] (R_s)	Δr in km Tadpole	Horseshoe	Chaos
Mimas	0.38±0.01	6.6×10^{-8}	185.52(3.075)	55	380(4500$^{\Delta}$)	2200
Enceladus^{++}	0.8±0.3	1.4×10^{-7}	238.02(3.945)	100	620(7400$^{\Delta}$)	3450
Tethys	7.6±0.9	1.3×10^{-6}	294.66(4.884)	390	1600(19000$^{\Delta}$)	8000
Dione	10.5±0.3	1.8×10^{-6}	377.40(6.256)	580	2300(27500$^{\Delta}$)	11000
Rhea	24.9±1.5	4.4×10^{-6}	527.04(8.736)	1300	4300(52000$^{\Delta}$)	20000
Titan	1345.7±0.3	2.36×10^{-4}	1221.8(20.25)	22000	38000(450000$^{\Delta}$)	150000
[F–ring moonlet^{+}		5×10^{-13}	140.18(2.32)	0.2	5.5(67$^{\Delta}$)	55

* From Burns (1986)

$^{+}$ Trajectories shown in Fig. 2–4

$^{++}$Trajectories shown in Fig. 5–7

$^{\Delta}$Longitudinal separation of maximum horseshoe y_{min}

FIGURE CAPTIONS

Fig. 1 The circular restricted three body problem as seen in a coordinate system that rotates with the satellite's orbital motion. L_i are the Lagrangian equilibrium points. Tadpole orbits lie within the curves enclosing the stable triangular Lagrange points L_4 and L_5, while horseshoe paths exist between the tadpole region and the nearly circular curves just inside and outside the satellite's orbit.

Fig. 2 As seen in a coordinate system that moves with the satellite [(located at (0,0)], trajectories of particles are plotted moving past a small satellite ($r \approx$ 5km, $\rho = 1.5 \text{g cm}^{-3}$) located on a circular orbit at 140, 180 km from Saturn. The various dynamical regimes are identified and the lengths of the approximate scalings of some regimes are shown. Figs. 3 and 4 are higher resolution versions. Note the distortion of y:x lengths.

Fig. 3 A higher resolution version of Fig. 2 where the cleared wake (upper right and lower left of satellite) is evident. The turning distance y_{min} for symmetric horseshoes as computed from $6\mu^{1/3}R$ is shown.

Fig. 4 A yet higher resolution version of Fig. 2.

Fig. 5 A plot of trajectories in the vicinity of Enceladus ($r \approx 250$ km, $\rho = 1.2$ g–cm^{-3}, on a circular orbit at R = 238,000 km) as seen in a coordinate system that is centered on Enceladus and rotates with it.

Fig. 6 A higher resolution version of Fig. 5.

Fig. 7 Particle positions are shown at equal time intervals for those orbits in Fig. 5 that did not strike the moon nor pass its longitude. Those orbits that approach the satellite most closely are splayed out following the interaction and their relative speeds are also increased. Thus horseshoeing particles will have relatively low spatial densities in regions inward/leading and outward/trailing the satellite.

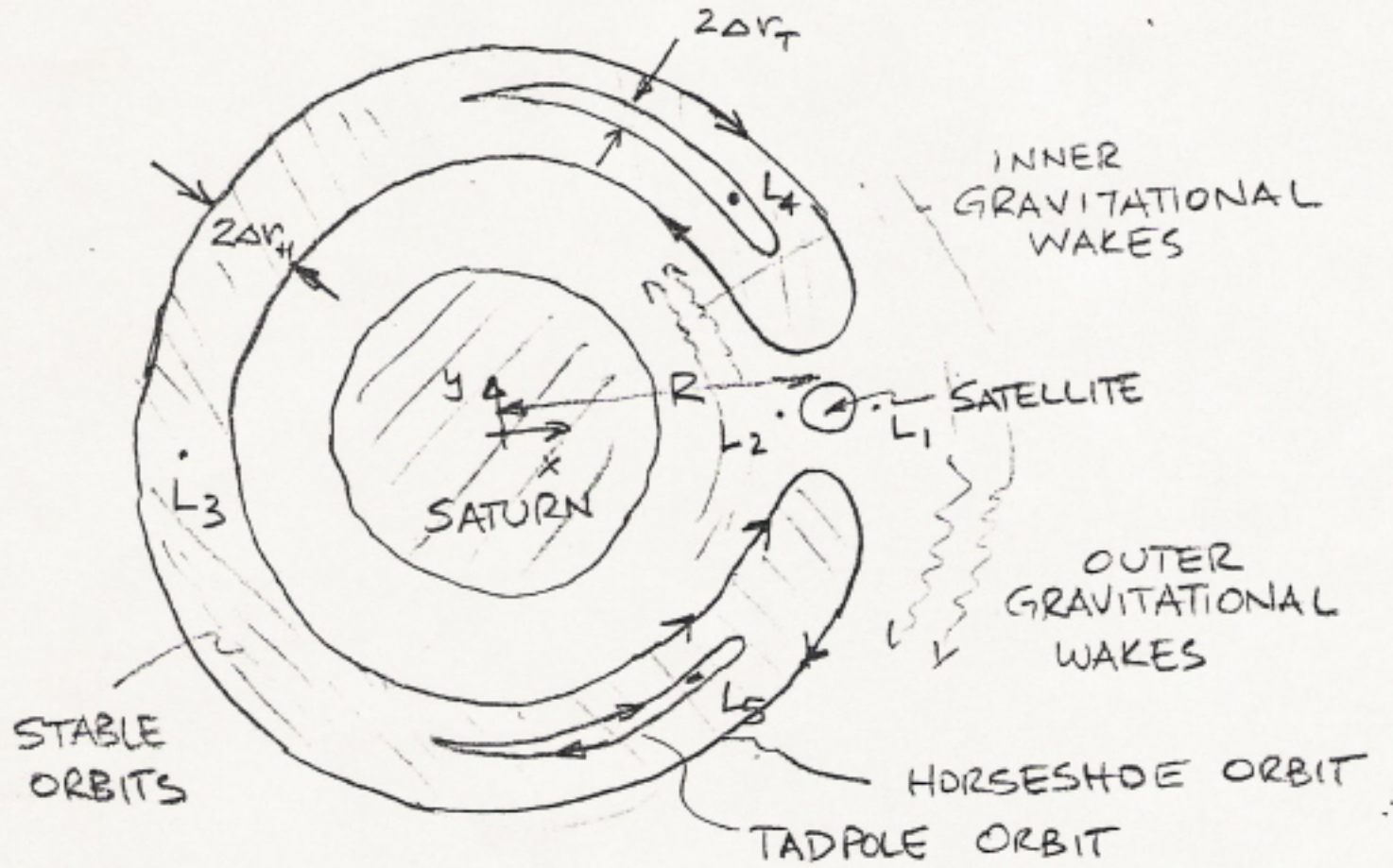
$2\Delta r_T$
$2\Delta r_H$
INNER GRAVITATIONAL WAKES
L_4
y
R
SATELLITE
L_2
L_1
L_3
SATURN
OUTER GRAVITATIONAL WAKES
L_5
STABLE ORBITS
HORSESHOE ORBIT
TADPOLE ORBIT

FIG. 1

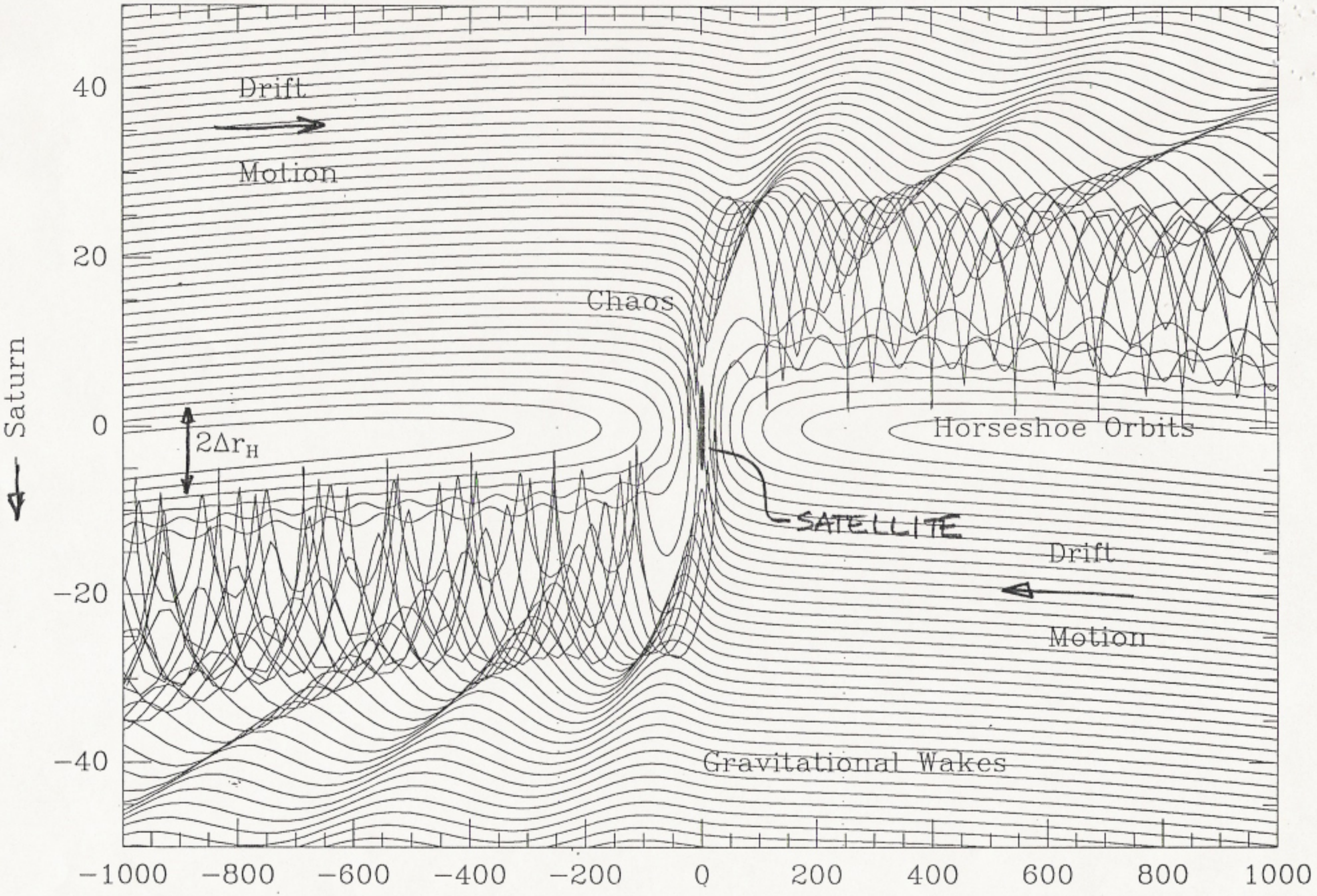
40
20
0
−20
−40
−1000
−800
−600
−400
−200
0
200
400
600
800
1000
Drift
Motion
Chaos
Horseshoe Orbits
$2\Delta r_H$
SATELLITE
Drift
Motion
Gravitational Wakes
Saturn

FIG.2

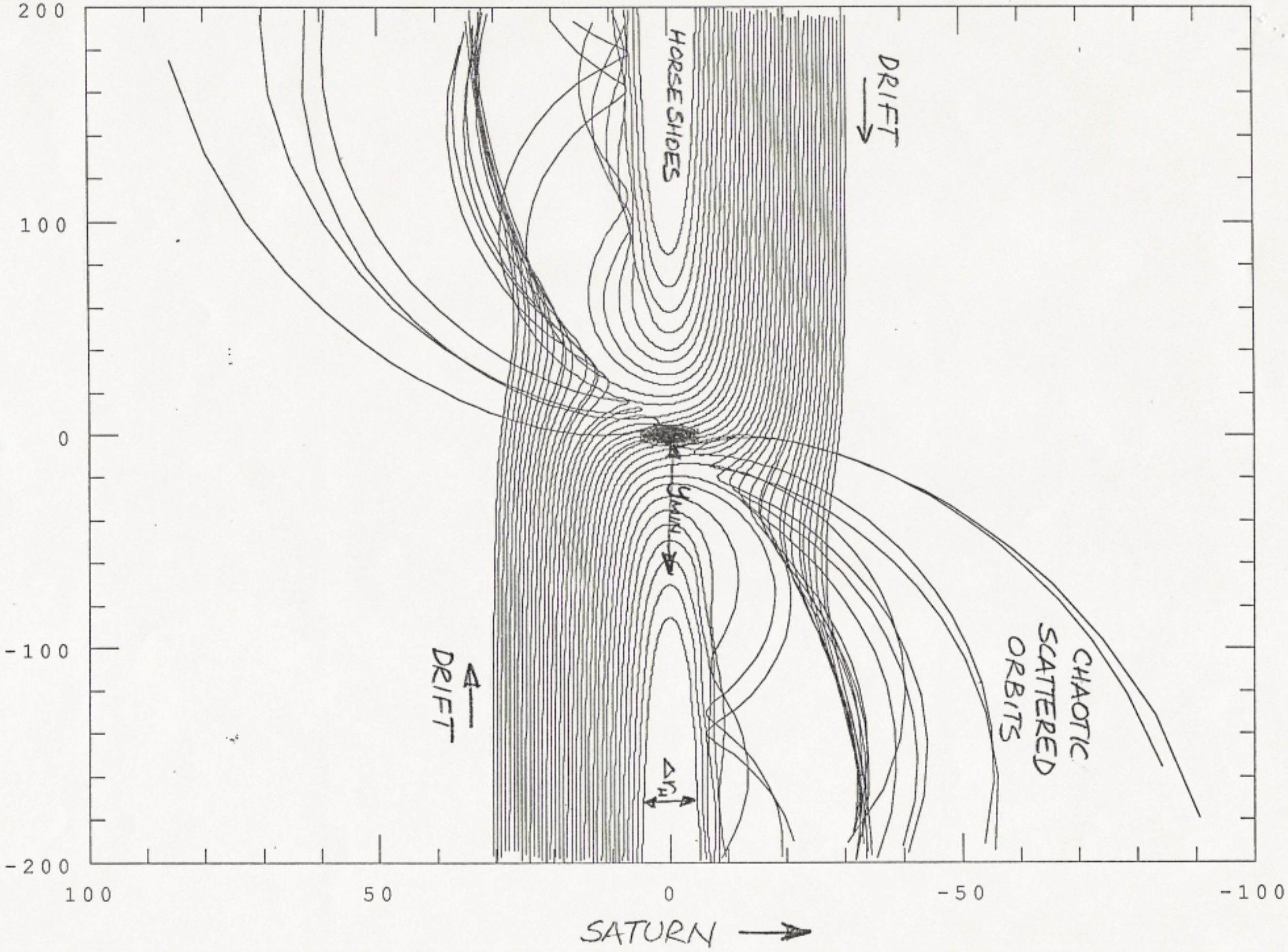
200
100
0
-100
-200
100
50
0
-50
-100
HORSE SHOES
DRIFT
y_{MIN}
DRIFT
Δr_H
CHAOTIC
SCATTERED
ORBITS
SATURN

FIG. 3

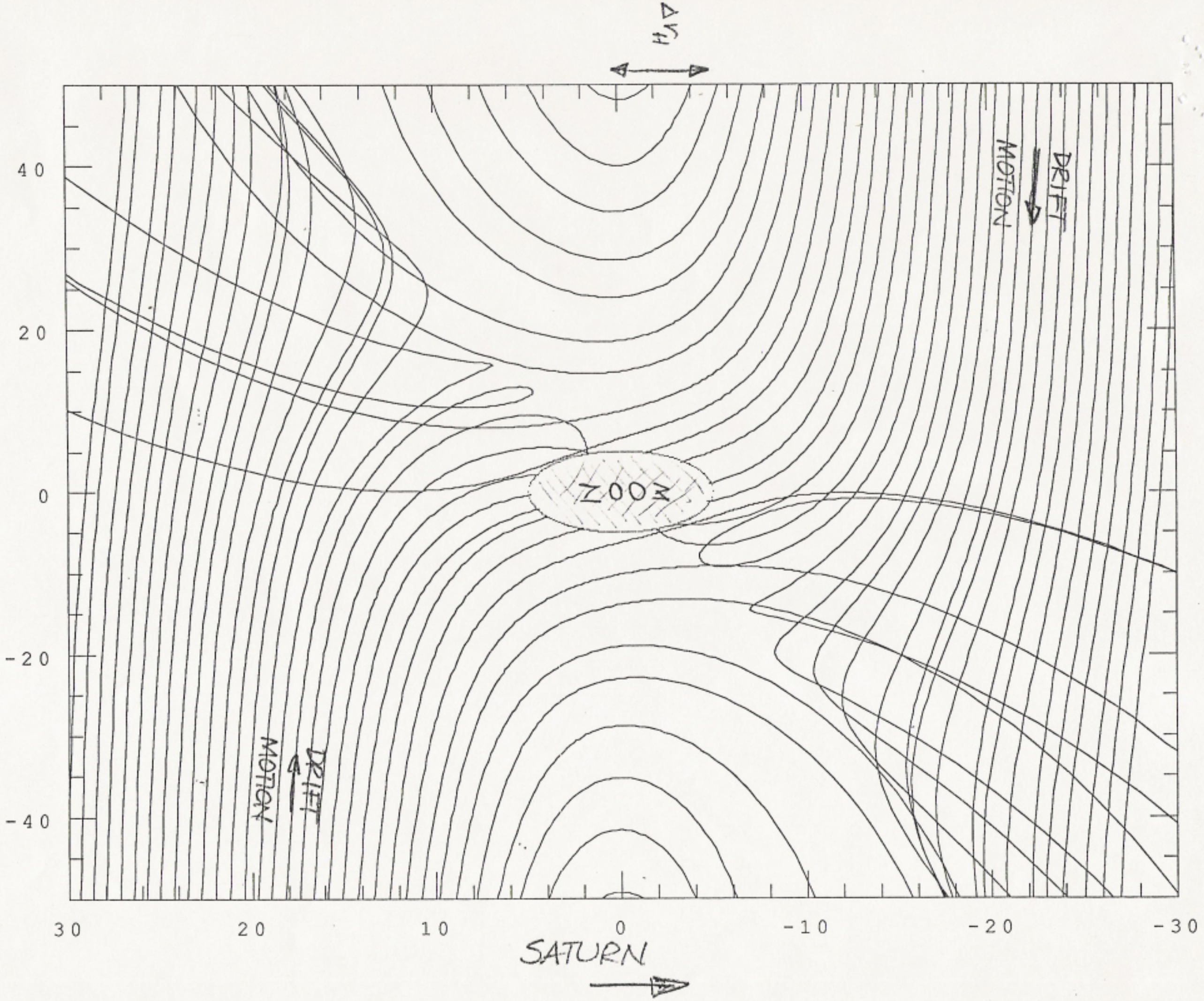

FIG. 4

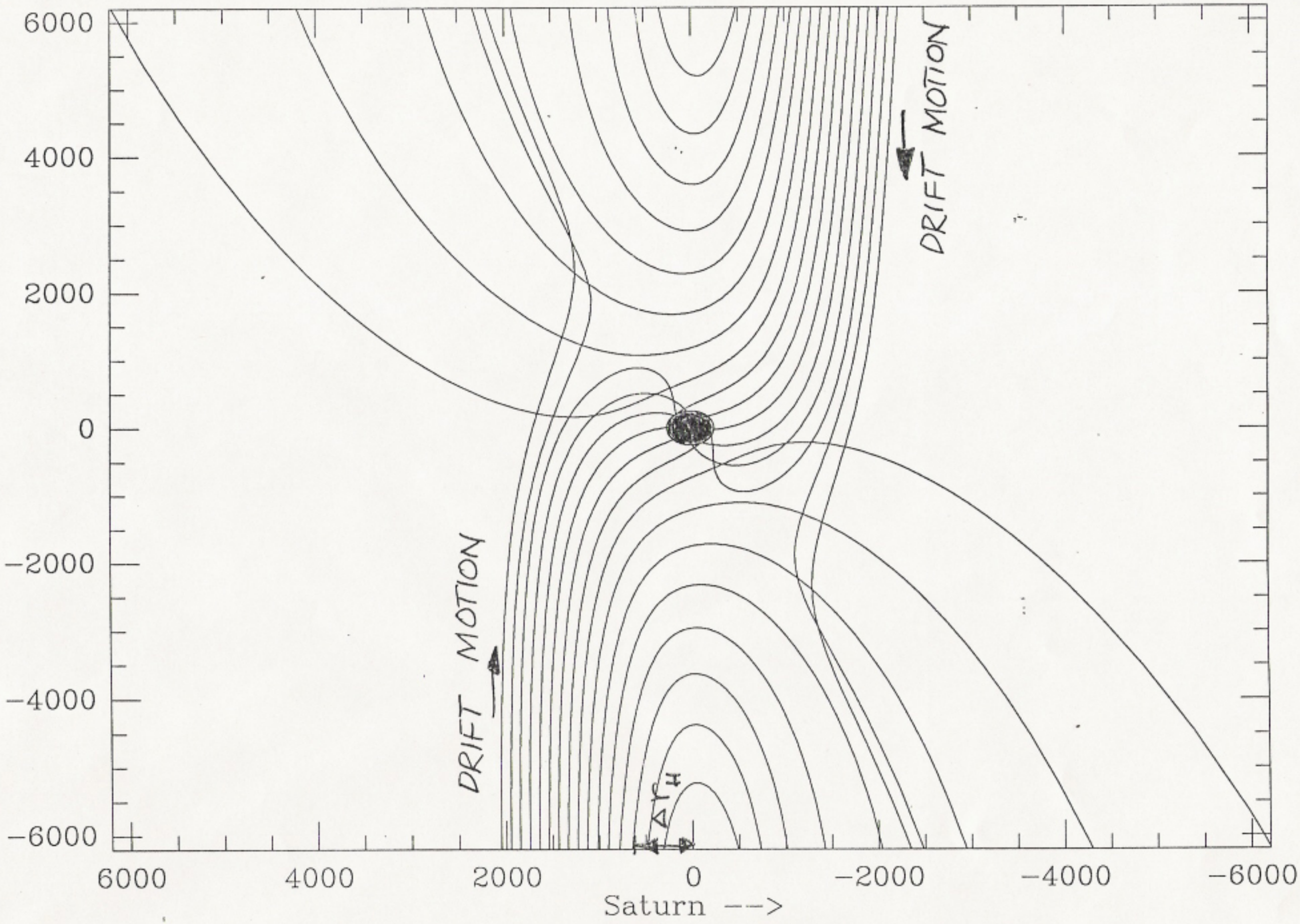
6000
4000
2000
0
−2000
−4000
−6000
6000
4000
2000
0
−2000
−4000
−6000
Saturn −−>
DRIFT MOTION
DRIFT MOTION
Δr_H

FIG. 5

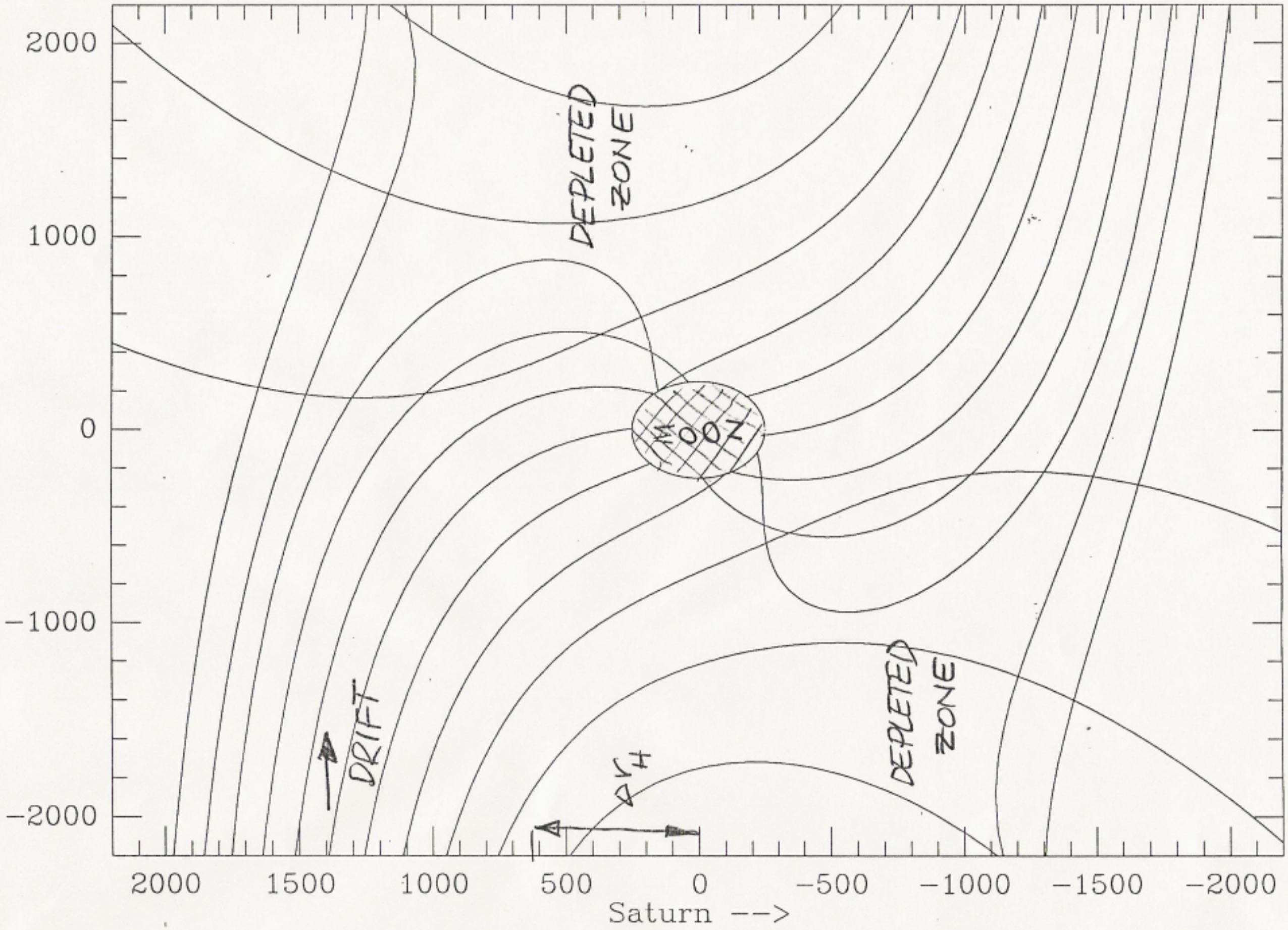
2000
1000
0
−1000
−2000
DEPLETED ZONE
MOON
DRIFT
Δr_H
DEPLETED ZONE
2000
1500
1000
500
0
−500
−1000
−1500
−2000
Saturn -->

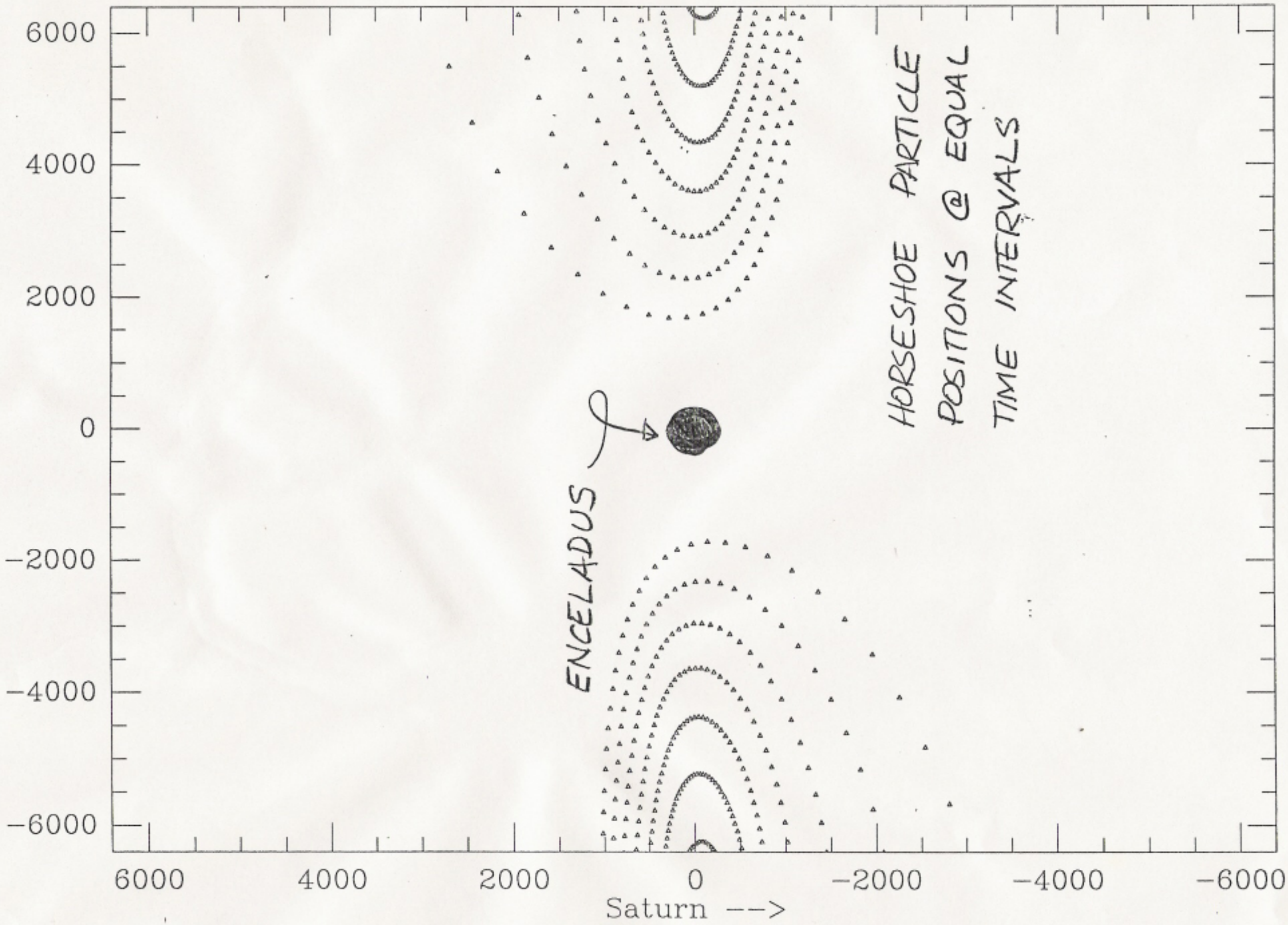
6000
4000
2000
0
−2000
−4000
−6000
6000
4000
2000
0
−2000
−4000
−6000
Saturn −−>
ENCELADUS
HORSESHOE PARTICLE
POSITIONS @ EQUAL
TIME INTERVALS

FIG. 7